First Experiment on Spectroscopy of Λ-Hypernuclei by Electroproduction at Jlab

L. Tang[1,10], T. Miyoshi[2], M. Sarsour[3], L. Yuan[1], X. Zhu[1], A. Ahmidouch[4], P. Ambrozewicz[5], D. Androic[6], T. Angelescu[7], R. Asaturyan[8], S. Avery[1], O.K. Baker[1], I. Bertovic[6], H. Breuer[9], R. Carlini[10], J. Cha[1], R. Chrien[11], M. Christy[1], L. Cole[1], S. Danagoulian[4], D. Dehnhard[12], M. Elaasar[13], A. Empl[14], R. Ent[10], H. Fenker[10], Y. Fujii[2], M. Furic[6], L. Gan[1], K. Garrow[10], A. Gasparian[1], P. Gueye[1], M. Harvey[1], O. Hashimoto[2], W. Hinton[1], B. Hu[1], E. Hungerford[3], C. Jackson[1], K. Johnston[15], H. Juengst[12], C. Keppel[1], K. Lan[3], Y. Liang[1], V.P. Likhachev[16], J.H. Liu[12], D. Mack[10], K. Maeda[2], A. Margaryan[8], P. Markowitz[17], J. Martoff[5], H. Mkrtchyan[8], T. Petkovic[6], J. Reinhold[17], J. Roche[18], Y. Sato[1,2], R. Sawafta[4], N. Simicevic[15], G. Smith[10], S. Stepanyan[8], V. Tadevosyan[8], T. Takahashi[2], H. Tamura[2], K. Tanida[19], M. Ukai[2], A. Uzzle[1], W. Vulcan[10], S. Wells[15], S. Wood[10], G. Xu[3], Y. Yamaguchi[2], and C. Yan[10]

1) Department of Physics, Hampton University, Hampton, VA 23668, USA
2) Department of Physics, Tohoku University, Sendai 980-8578, Japan
3) Department of Physics, University of Houston, Houston, TX 77204, USA
4) Department of Physics, North Carolina A&T State University, Greensboro, NC 27411, USA
5) Department of Physics, Temple University, Philadelphia, PA 19122, USA
6) University of Zagreb, Zagreb, Croatia
7) University of Bucharest, Bucharest, Romania
8) Yerevan Physics Institute, Yerevan, Armenia
9) Department of Physics, University of Maryland, College Park, MD 20742, USA
10) Thomas Jefferson National Accelerator Facility, Newport News, VA 23606, USA
11) Brookhaven National Laboratory, Upton, NY 11973, USA
12) Department of Physics, University of Minnesota, Minneapolis, MN 55455, USA
13) Department of Physics, Southern University at New Orleans, New Orleans, LA 70126, USA
14) Department of Physics, Rensselaer Polytechnic Institute, Troy, NY 12180, USA
15) Department of Physics, Louisiana Tech University, Ruston, LA 71272, USA
16) Institute of Physics, University of Sao Paulo, Sao Paulo, Brazil
17) Department of Physics, Florida International University, Miami, FL 27411 USA
18) Department of Physics, College of Williams and Mary, Williamsburg, VA 23187, USA
19) Department of Physics, University of Tokyo, Tokyo 113-0033, Japan

Abstract. The first experiment in Λ-hypernuclear spectroscopy using the high-precision electron beam at Jefferson laboratory (JLab) has been carried out. The hypernuclear spectrometer system (HNSS) was used to measure spectra from the ^{12}C(e, e′K$^+$)$^{12}_{\Lambda}$B reaction with sub-1-MeV resolution, the best energy resolution obtained thus far in hypernuclear spectroscopy with magnetic spectrometers. This paper describes the HNSS and the preliminary results for the $^{12}_{\Lambda}$B system. The experimental spectrum is consistent with the expected strong spin-flip

excitations of unnatural parity states. A program of hypernuclear physics experiments is planned for the future with much higher yield and even better energy resolution.

1. INTRODUCTION

The introduction of a new degree of freedom, strangeness, into the nuclear medium challenges our conventional models of the nuclear many-body system to their limits. Many new features of the strong interaction between hyperons and the nuclear medium and between hyperons and nucleons can be explored[1]. Analyses of experiments on light and heavy systems[2,3,4,5,6] have shown that the Λ particle, because it is distinguishable from nucleons, can indeed occupy any of the nuclear shells, even those filled with nucleons. Thus, the Λ can be used as an effective probe of the nuclear interior. In addition, the knowledge of an effective hyperon-nucleus interaction deduced from such studies will enable the extraction of an effective ΛN interaction that is difficult if not impossible to obtain by others means.

Traditionally, hypernuclear studies have been carried out using secondary hadronic beams (K or π mesons), producing the Λ in the nucleus by a strong interaction with a nucleon. Fig. 1(a) is a simplified illustration of these processes. For the (K^-, π^-) reaction the momentum transfer is small and the cross section is relatively large. The spectroscopy is characterized predominantly by the excitation of low-spin substitutional states[7,8] where the Λ replaces the nucleon in the same shell model orbit. For the (π^+, K^+) reaction the momentum transfer is large and the cross section is relatively small[2]. This reaction preferentially populates high-spin stretched states[2,3] where a nucleon hole is coupled to a Λ. Because the Λ can be in any shell this reaction also produces deeply bound states with the Λ in the s-shell. At forward angles, neither of the two reactions has significant spin-flip amplitude so that the spectra are dominated by the transitions to the states of natural parity.

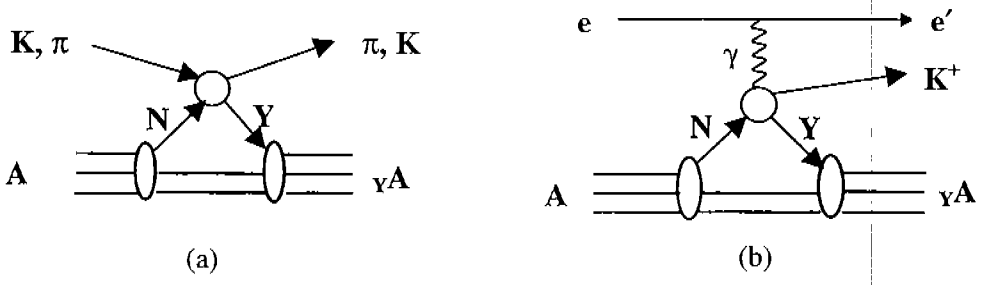

FIGURE 1. Comparison of the production processes: (a) hadronic and (b) electromagnetic.

The investigations using hadronic production have been hampered by poor energy resolution. Thus far, the best resolution (better than 2 MeV (FWHM)) with magnetic spectrometers was obtained in a study of light Λ-hypernuclei at KEK using the (π^+, K^+) reaction[9]. This work demonstrated the importance of good resolution in gaining significantly new information. Much better resolution than in experiments with magnetic spectrometers alone has been achieved in experiments detecting the ejected K^+ or π^- in a magnetic spectrometer in coincidence with γ's from hypernuclear decay using high-resolution Germanium crystals[10,11]. However, such studies are limited to

particle stable states. Thus there is continued interest to obtain better and better resolution in experiments that measure single spectra of the residual nucleus excited to either particle bound or unbound states. High resolution is of special importance for extracting parameters of the spin-dependent Λ-nucleus interaction and for studying the single particle motion of the Λ in the strongly interacting nuclear medium[12].

Electroproduction of hypernuclei using a high-duty factor (100%) and high-intensity electron beam, such as the CEBAF beam at JLab, has long been known for its many unique features[13] that deserve to be exploited. In Fig. 1 we compare the diagram (1b) for the electroproduction process, $A(e, e'K^+)_Y A$, with that (1a) for the hadronic processes. Here the subscript Y indicates a hyperon in the nucleus. The electro-magnetic process with an exchange of a colorless virtual photon is much better understood theoretically than the strong process. Even at far forward angles the spin-flip amplitude is large in contrast to the hadronic process where the spin-flip amplitude is small. The momentum transfer is high ($q \geq 300$ MeV/c), similar to that of the (π^+, K^+) reaction. Therefore, the spectra are expected to show strong spin-flip transitions to high-spin stretched states of unnatural parity as well as transitions to natural parity states and to deeply bound states.

The very different features of the different reactions make it possible to study a large variety of hypernuclear states[14]. In addition, the electromagnetic process changes a proton in the nucleus into a Λ, creating a proton-hole—Λ-particle state whereas the frequently studied hadronic reactions change a neutron into a Λ resulting in a neutron-hole—Λ-particle state. For targets of equal number of neutrons and protons, the reactions induced by the electromagnetic and hadronic processes lead to mirror Λ hypernuclei thus allowing studies of charge symmetry breaking in the effective Λ-nucleon interaction.

Cross sections for electromagnetic production are at least two orders of magnitude smaller than that for hadronic processes, but this can be compensated by much higher beam intensity. Due to the high quality of the primary electron beam and the ability to transport it to the target without losing its high precision, there is no need for tracking the incident electrons. Energy and angle straggling in the target are minimized by use of a very thin target. Estimates show that it should be possible to reach an energy resolution in the sub-1-MeV range. (See below). With such precision, the $(e, e'K^+)$ reaction is a powerful probe for a systematic study of hypernuclei.

2. HNSS EXPERIMENT

JLab experiment E89-009, employing the HNSS, is the first high-resolution hypernuclear spectroscopy experiment using electromagnetic production of strangeness. This experiment probes certain expectations for electroproduction of hypernuclei and tests our experimental techniques.

2.1 Experimental Considerations

In electroproduction, the Λ and K^+ particles are created associatively via an interaction between a virtual photon and a proton in the nucleus. The hypernucleus $_Y A$

is formed by coupling the Λ to the residual nuclear core, as shown in Fig. 1(b). The energy and momentum of the virtual photon are defined as $\omega = E\text{-}E'$ and $\mathbf{k} = \mathbf{p}\text{-}\mathbf{p}'$, respectively. The four-momentum transfer of the electron is then given by $Q^2 = k^2\text{-}\omega^2$. Since the elementary cross section for $p(e, e'K^+)\Lambda$ falls off fast with increasing Q^2, the measurements should be done at Q^2 close to zero. This requires that the electron scattering angle should be as small as possible.

To a good approximation, the electroproduction cross section can be expressed[15] by

$$\frac{d^5\sigma}{dE'd\Omega'd\Omega_K} = \Gamma\frac{d^2\sigma}{d\Omega_K}, \qquad (1)$$

where Γ is the integrated virtual photon flux produced by (e, e′) scattering and $d^2\sigma/d\Omega_K$ is the photoproduction cross section. As $Q^2 \rightarrow 0$, the cross section is completely dominated by the transverse component.

For the current experiment ω was chosen to be about 1.5 GeV, at which the elementary photoproduction cross section has its maximum. In order to keep the rate of events from background K^+ production channels small, the energy (E) of the incident electrons was set to about 1.8 GeV. Thus, the scattered electron energy (E′) was about 0.3 GeV. Fig. 2 shows the calculated virtual photon flux factor in units of photons per electron per MeV per sr for the chosen kinematics. This factor is peaked near zero degrees and falls off rapidly as the scattering angle increases. With the electrons detected at zero degrees, even a relatively small solid angle will accept a large percentage of the scattered electrons. Thus, the chosen experimental parameters simplify the electron detection and maximize the virtual photon flux. However, near zero degrees the electron background rate from bremsstrahlung increases even faster with decreasing angle than the virtual photon flux so that the electron single-arm rate is dominated by electrons from bremsstrahlung thus limiting the usable luminosity of the beam.

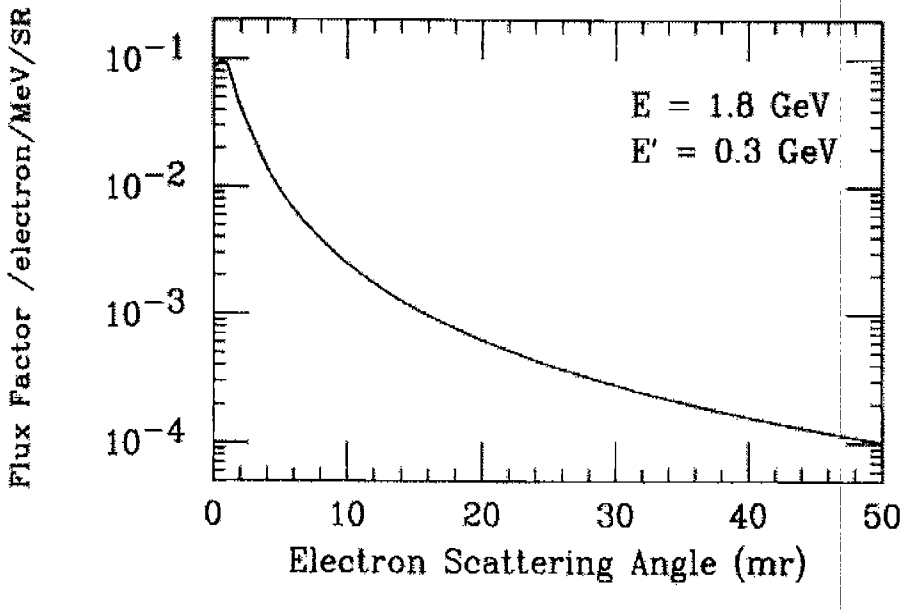

FIGURE 2. Virtual photon flux factor as a function of electron scattering angle.

In the (e, e′K^+) reaction, both the scattered electron and the K^+ have to be detected in coincidence. With the kinematics chosen for the electron scattering, the K^+ momentum is about 1.2 GeV/c. The 3-momentum transfer to the associatively produced Λ is about q $\approx$ 300 MeV/c when the K^+ is detected at zero degrees. The production cross sections for the hypernuclear ground state and core-excited states decrease strongly as the 3-momentum increases with the K^+ scattering angle. One advantage of using low incident electron and scattered electron energies (about 1.8 and 0.3 GeV, respectively,) is that the cross sections drop more slowly in the small forward angle region since the 3-momentum increases more slowly than in the case of higher electron energies. Thus, detecting the K^+ at angles near zero degrees ensures maximization of hypernuclear production. The relatively large momentum transfer to the Λ, similar to that of the (π^+,K^+) reaction, provides access to deeply bound and high-spin states.

2.2 Experimental Setup

Fig. 3 shows a schematic top view of the HNSS. In order to be able to detect both scattered electrons and positively charged kaons near zero degrees a "C" dipole, placed right behind the experimental target, served as a beam splitter. It bent the scattered electrons (centered at zero degrees) and the kaons (centered at about 2 degrees) in opposite directions by 33 and 16 degrees, respectively. The target was located at the effective field boundary of the splitter magnet.

The scattered electrons were detected by a split-pole magnetic spectrometer[16]. The central momentum of the spit-pole spectrometer was chosen to be 300 MeV/c where its momentum acceptance is about 120 MeV/c. The solid angle acceptance of the combined splitter and split-pole system was about 9 msr, which effectively tagged about 35% of the virtual photon flux within the momentum acceptance. This was possible because of the far forward peaking of the scattered electrons mentioned above. The momentum of the scattered electrons was then simply a function of the position in the momentum dispersion plane.

In order to be able to handle the very high rates of scattered electrons and to keep the means of detecting the electrons simple, the focal plane detector for the split pole was made of 10 one-dimensional silicon strip detectors (SSD) with 144 strips each and a pitch width of 0.5 mm. The 10 SSD cover the full length of the 72-cm long focal plane. The position measurement provided directly the momentum of the scattered electron. Eight scintillation strip counters were placed behind each of the 10 SSD, a total of 80 strips. They were used to provide the timing for the coincidence with the kaons.

The kaons were detected by an existing short orbit spectrometer (SOS) placed so that the kaon scattering angle centered at 2 degrees. The angular acceptance of the SOS was about 6 msr covering a range of scattering angles from 0 to 4 degrees. The central momentum was set at 1.2 GeV/c and the acceptance was about 46%. Only the central $\pm$15% of the acceptance was used where it is flat within the range of missing mass of interest. The total path length of the kaons from the target to the end of the SOS detectors was 10 m. Thus, on the average the survival rate from target to focal area was 35%.

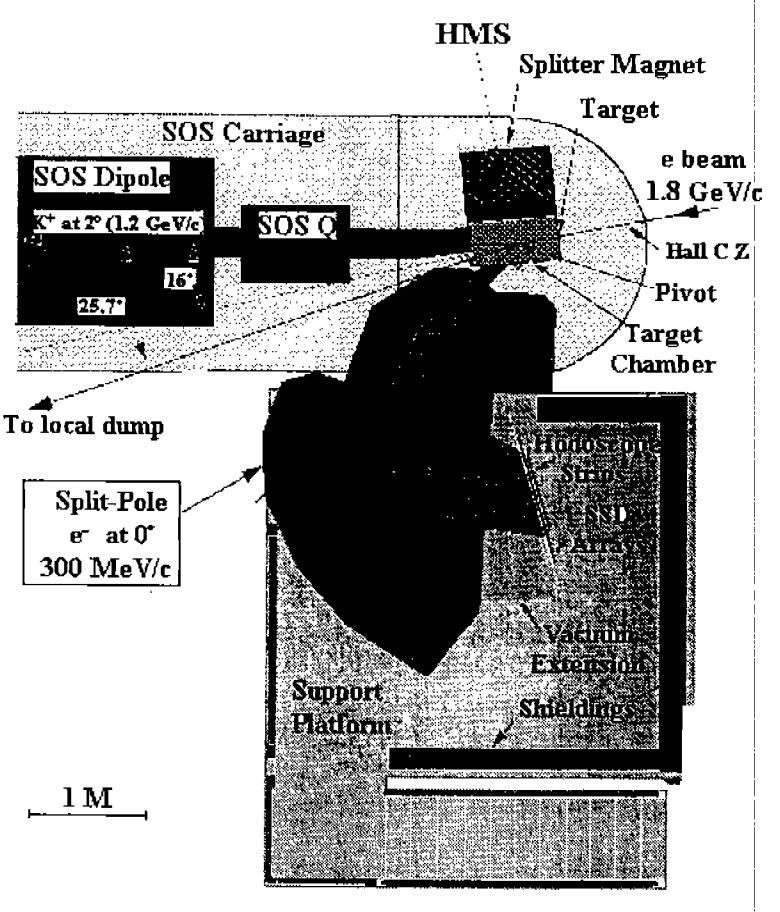

FIGURE 3. Top view of the layout of the HNSS.

The standard SOS detector system was used for kaon detection. It consists of: (1) two sets of tracking chambers that measure positions and angles at the focal plane for momentum reconstruction, (2) four scintillation hodoscope planes to provide coincidence timing to the electron arm and also to measure the time-of-flight (TOF) for separation of kaons and background particles (p, π^+, and e^+), (3) one aerogel Čerenkov (AČ) veto counter to reduce π^+ and e^+ background triggers, (4) one Lucite Čerenkov (LČ) counter to reduce the proton triggers, and (5) one gas Čerenkov (GČ) detector and 3 layers of shower counters to reject the e^+ triggers.

The JLab beam has a bunch width of 1.67 ps and a separation between bunches of 2 ns. The coincident time resolution for the two arms was $\sigma \approx 400$ ps after path length and signal size corrections for both arms. This resolution was sufficient to identify the real and accidental coincidence peaks individually in the coincidence time spectrum. The final e'/K^+ coincidence events were selected by a two-dimensional cut on the real coincidence window of 2 ns and the velocity measurement (from TOF in the SOS). The events selected from eight nearby accidental coincidence windows were used to obtain the shape and magnitude of the accidental background spectra to high accuracy (see below).

Three different thin target foils were employed, CH_2, ^{12}C, and ^{7}Li. The CH_2 foil (100 μm thick) was used for calibration and optical tuning using events from the $p(e,e'K^+)\Lambda$ reaction. $^{12}_{\Lambda}B$ and $^{7}_{\Lambda}He$ hypernuclear spectra were obtained from the ^{12}C (22 mg/cm^2) and ^{7}Li (19 mg/cm^2) targets. In the HNSS, a complete vacuum system coupled the beam line, target chamber, and spectrometers. Thus multiple scattering in vacuum windows happened only in the exit windows of the spectrometers where multiple scattering effects were minor since these foils were located right in front of the first tracking detector. Table 1 lists the sources of contributions to the energy resolution and the expected overall energy resolution for this experiment. The SOS contribution was expected to dominate.

TABLE 1. Sources of Contribution and Expected Overall Energy Resolution for HNSS.

Source	Contribution	Resolution (keV) (FWHM)
Beam Energy Uncertainties	$\leq 10^{-4}$	≤ 180
SOS momentum Uncertainty	$\leq 5\times10^{-4}$	≤ 600
e′ Arm Momentum Uncertainty	$\leq 5\times10^{-4}$	≤ 150
K^+ Scattering Angle Uncertainty	10 mr	≤ 200 (^{12}C)
Target Energy Loss Uncertainty	1.7 keV/mg/cm^2	38 (^{12}C)
Total		≤ 678

2.3 Rates, Background, and Calibrations

The single rate in the electron arm reached about 2×10^8/sec. It was primarily due to background of bremsstrahlung electrons that cannot be distinguished from the coincident electrons. Therefore, the experiment used the much less frequent kaon arm events in the trigger. Coincidence spectra were obtained later in off-line analysis. The high electron rate caused large accidental background in the spectra. The SSD and scintillation hodoscopes worked well under the high rates.

The positrons from e^+/e^- pair production that were emitted near zero degrees dominated the kaon arm single rate. Since the SOS covered an angular range from 0 to 4 degrees, these positrons were accepted by the SOS but the combined use of vetoes from AČ, GČ, and shower counters eliminated this background. The rate from background protons and π^+'s were low (~1 kHz) after on-line rejection by the AČ and LČ detectors. The remaining background protons and π^+'s were eliminated in off-line analysis using TOF information.

Due to the high rate in the electron arm, about 95% of the background in the spectra was from accidental coincidences. A precise measurement of this background was obtained as follows. The analysis of the raw data generates a spectrum of the time difference between the emission of the K^+ and the electron from the target. In addition to a peak corresponding to the true coincidences there are many peaks containing only accidental coincidences, 2 ns apart according to the time structure of the electron beam. The analysis of the events from the accidental coincidence peaks in the time spectrum under the same condition as those from the real coincidence peak provided a high-statistics background spectrum that could be subtracted from the missing-mass spectrum (containing the real and the accidental coincidences) after proper normalization. The remainder of the background (5%) was from the real coincidences

with π^+'s. The full path length TOF separation between π^+'s and K^+'s was 2 ns. Therefore the real coincidental π^+'s should be contained in a coincident peak next to the real K^+ coincidences according to the beam bunch structure. The timing resolution of $\sigma \approx 400$ ps allowed an overlap of the tails from the real K^+ and π^+ coincidence peaks. The magnitude of this background was determined by analyzing the overlap. The shape of the background in the missing-mass spectra was then obtained by an analysis of the coincident π^+ assuming (e, e′K^+) kinematics. The absolute magnitude of the background was obtained by normalizing the spectrum to the number of background events in the spectrum.

An upper limit for the HNSS resolution was obtained by investigating the coincident events of the A(e, e′ e^+e^-)A reaction. The beam energy was reconstructed simply by a summation of the energies of the two electrons (the scattered electron e′ and the electron from pair production) in the electron arm and a positron (from the pair production) in the SOS. The result is shown in Fig. 4. This method includes the contributions to the resolution from the extra electron in the split pole that does no exist in the (e′K^+) final state. The 820-keV (FWHM) resolution in Fig. 4 is therefore an upper limit of what we expect for the missing mass spectra from the (e, e′K^+) reaction.

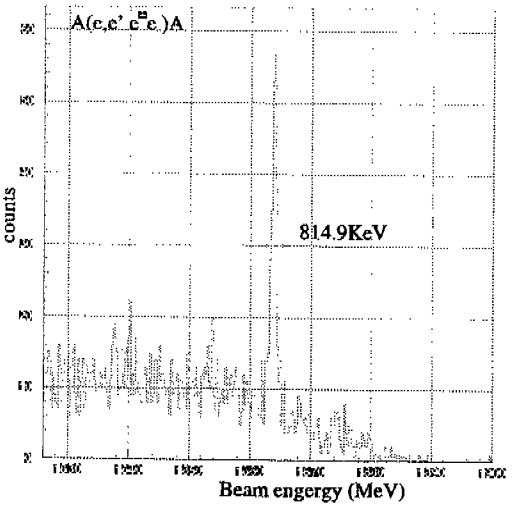

FIGURE 4. Reconstructed beam energy, which provided the upper limit of the HNSS resolution.

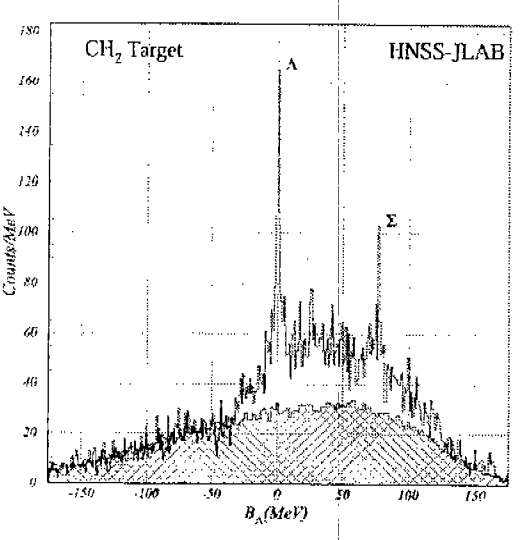

FIGURE 5. Missing mass spectrum with Λ and Σ^0 peaks from the p(e, e′K+) reaction using the CH_2 target.

Fig. 5 shows a missing mass spectrum obtained with the CH_2 target. The (e, e′K^+) reaction on the protons in the target produced both Λ and Σ^0. On the missing mass scale the mass of the Λ was subtracted which places the "missing mass" of the Λ at 0 MeV and that of the Σ^0 at 77 MeV. The shaded area is the background from the accidentals. The broad distribution above the accidental background other than the two peaks are events from the carbon in the CH_2 target. The beam was defocused to 4x4 mm^2 by the fast raster for the beam position on target and was kept below 1.5 μA to avoid target melting. The peak width (FWHM) of the hyperon peaks is about 3

MeV. This large width is due to the kinematic broadening within the angular resolution (10 mr) of the SOS for the scattered kaons and the large beam size. This broadening effect is much smaller (<200 keV) for the carbon target.

The missing mass scale, which depends on the beam energy and the central momenta of both electron and kaon arms, was calibrated using the measured positions of the Λ and Σ^0 peaks and their known masses. The systematic error from this calibration in the determination of the binding energy of the hypernuclear system is about 125 keV. This error is mainly due to the low statistics in the Λ and Σ^0 peaks. The width of the peaks has no effect on the calibration. The spectrum of Fig. 5 also provides a first measurement of the cross section of the electroproduction of hyperons on protons near $Q^2 = 0$.

3. EXPERIMENTAL RESULT

The HNSS experiment obtained data for both $^{12}_{\Lambda}$B and $^{7}_{\Lambda}$He hypernuclei using ^{12}C and ^{7}Li targets. Our analysis is currently focusing on $^{12}_{\Lambda}$B. Fig. 6 shows a preliminary missing mass spectrum of the $^{12}_{\Lambda}$B hypernucleus, plotted in terms of the Λ binding energy with the background (shaded area) included. The background spectrum of accidentals (≈95% of all background) was obtained with very good statistics using events from eight accidental coincidence peaks. The remaining background (about 5%) was from a contamination by real coincident π^+'s, as mentioned previously. The high accidental rate was from the bremsstrahlung electrons that are peaked strongly at zero degrees. This high rate not only limited the maximum usable luminosity and thus the good event rate. Fig. 7 shows the spectrum with the background subtracted and with half the bin size of the spectrum in Fig. 6. The error bars are the statistical errors with the contribution from the background subtraction included.

Only specific hypernuclear states are expected[14,17] to have significant strength in the (e, e′K^+) reaction, whereas others may be strongly excited in the (π^+, K^+) or (K^-, π^-) reactions. In our preliminary spectrum the most prominent peak, located at $B_\Lambda \approx -11.5$ MeV, is from the transition to the ground state doublet of $^{12}_{\Lambda}$B. This unresolved ($1^-_1/2^-_1$) doublet is made primarily by coupling a Λ in the s shell to the ground state of ^{11}B (primarily a proton hole in the $p_{3/2}$ shell). The 2^- state can be reached only by spin-flip of Λ and is thus expected to be more strongly excited by the (e, e′K^+) reaction than the 1^- state. Theory predicts a spacing between the two states (resulting from spin-dependent parts of the interaction) of roughly 100 keV, too close to be resolved in our experiment. We note that in the study[9] of the ^{12}C(π^+, K^+) reaction the 1^- state of the g.s. doublet in the mirror hypernucleus $^{12}_{\Lambda}$C is the most strongly excited state. The second clearly visible peak, at $B_\Lambda \approx -5.9$ MeV, we tentatively interpret to be the predicted 2^-_3 state arising from coupling the Λ in the s shell to the first excited $3/2^-$ state of the ^{11}B core. This 2^-_3 state is also a member of a ($1^-/2^-$) doublet with its 1^- member observed in the (π^+, K^+) reaction.

There is an indication of a peak at $B_\Lambda \approx -8.9$ MeV, between the other two s- shell Λ states mentioned above, where the 1^-_2 state of a ($0^-/1^-$) doublet, made by ($p_{1/2}^{-1}$, s^Λ) coupling, is expected but the statistics is not sufficient to make a solid claim.

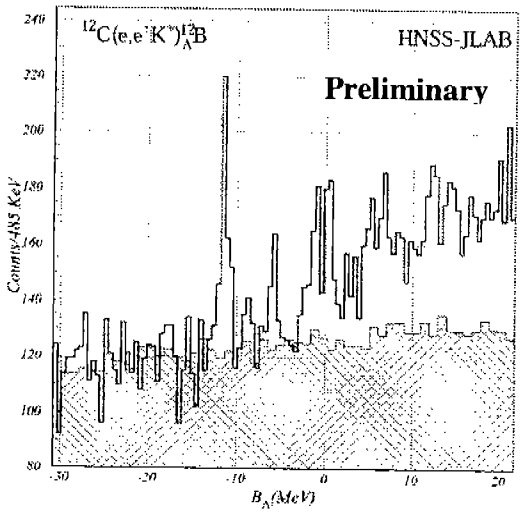

FIGURE 6. Preliminary $^{12}_{\Lambda}$B missing mass spectrum including background.

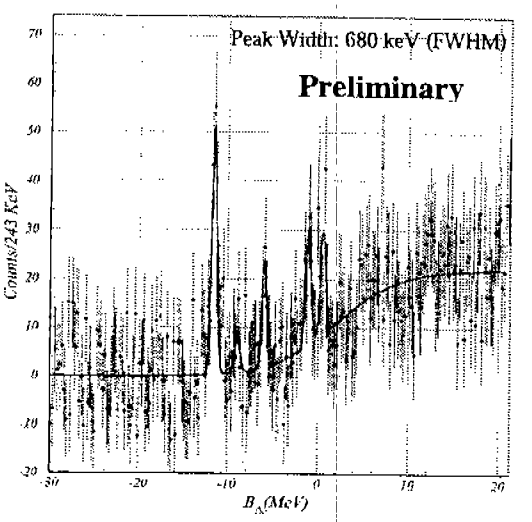

FIGURE 7. Background-subtracted $^{12}_{\Lambda}$B spectrum. Five peaks are fitted with a common peak width.

Near breakup threshold, between B_Λ = -2 and +1 MeV, several states arising from coupling a Λ in the $p_{3/2}$ shell to the $3/2^-$ g.s. of ^{11}B are expected. These are positive parity states of spin/parity 0^+, 1^+, 2^+, and 3^+, of which the 3^+ unnatural parity state is predicted to be most strongly excited and the 2^+ to contain about half the strength of that of the 3^+ state. It is not clear whether we can speak of two resolved peaks here. But the yield between B_Λ = -2 and +1 MeV must contain the predicted strongly excited 3^+ and 2^+ states.

Configuration mixing of the ^{11}B core states of the p shell hypernuclear states is expected to be significant[17]. This leads to the splitting of the total strength among many states. Nevertheless, theory predicts that a large fraction of the strength resides in the 3^+_1 state. The complex of states near breakup threshold is of great interest and will be the subject of more detailed investigation.

The experimental spectrum in Fig. 7 is the result of subtracting the background indicated in Fig. 6 by the shaded area from the total spectrum. Note that the bin size in Fig, 7 (243 keV) is half that of Fig. 6. The region from B_Λ = –30 to +20 MeV was fitted assuming five states and a background primarily from quasifree Λ production. The extracted peak positions are listed in Table 2 for a comparison with the most recent structure prediction provided by Millener[17]. The prediction lists all possible states from the coupling of a Λ to ^{11}B core states. The energies of the levels for the states with the Λ in the p shell had been given[16] relative to the lowest 2^+_1 state. In order to facilitate the comparison between experiment and theory, an energy separation of 10.69 MeV between the ground state and the 2^+_1 state was added to the theoretical values. 10.69 MeV had been reported as the excitation energy of the 2^+_1 state in $^{12}_{\Lambda}$C observed in the study[9] of the (π^+, K$^+$) reaction. We use this value for the 2^+_1 mirror state in $^{12}_{\Lambda}$B since the difference between the ^{11}C and ^{11}B core states is small. The extracted experimental values are listed in the table next to the closest theoretical values for comparison only. It does not mean an actual claim of experimental observation of a predicted state. Full interpretation of the experimental

spectrum will have to rely on detailed and complete theoretical studies. The uncertainty of the binding energy is dominated by the uncertainty in the missing mass scale calibration using the positions of the Λ and Σ^0 peaks in the relatively low-statistics spectrum from the CH_2 target.

TABLE 2. Comparison of Theoretically Predicted[17] and Preliminary Experimental Values.

State	Core State in ^{11}B	E_x (MeV) Theory	E_x (MeV) Experiment	B_Λ (MeV) Experiment
1^-_1 (Λ_s)	$3/2^-_1$	0.000		
2^-_1 (Λ_s)	$3/2^-_1$	0.165	#1 0.00	-11.53 ± 0.13
1^-_2 (Λ_s)	$1/2^-_1$	2.728	(#1' 3.06)	(-8.47 ± 0.13)
0^-_1 (Λ_s)	$1/2^-_1$	2.752		
2^-_2 (Λ_s)	$5/2^-_1$	4.553		
2^-_3 (Λ_s)	$3/2^-_2$	5.829	#2 5.62	-5.91 ± 0.13
1^-_3 (Λ_s)	$3/2^-_2$	5.894		
2^+_1 (Λ_p)		10.69	#3 10.43	-1.10 ± 0.13
1^+_1 (Λ_p)		10.72		
2^+_2 (Λ_p)		11.15		
3^+_1 (Λ_p)		11.23	#4 11.85	0.32 ± 0.13
0^+_1 (Λ_p)		11.31		
1^+_2 (Λ_p)		11.75		
2^+_3 (Λ_p)		13.00		
1^+_3 (Λ_p)		13.09		
1^+_4 (Λ_p)		13.37		

4. A NEW HNSS

From the current experiment we attained valuable information for planning future spectroscopic studies using the (e, e'K^+) reaction with a much-improved experimental setup. Fig. 8 shows the layout of a new generation experiment that has been proposed to and approved by the JLab program advisory committee[18]. The electron arm of the HNSS will be placed at an angle with respect to the floor plane so that the tagging angle of the scattered electrons is about 2.5 degrees. This will reduce the rate of forward electrons from bremsstrahlung by almost four orders of magnitude whereas the virtual photon flux will be reduced only by a factor of about 10. Thus, the new geometry allows a luminosity increase of more than a factor of 200. A new high-resolution and short-path-length kaon spectrometer (HKS) will be built. It is dedicated to the (e,e'K^+) hypernuclear spectroscopy program at JLab under the construction fund by Monkasho[19] of Japan. It will improve the kaon arm momentum resolution by a factor of two and its solid angle acceptance by a factor of about 3. Overall, the yield is expected to increase by a factor of about 50 and the energy resolution may reach 350 keV (FWHM). Finally, the background will be reduced by a factor of 10. The goal of the new experiment is to carry out high precision and high statistics studies on medium mass hypernuclei, e.g. $^{28}_{\Lambda}$Al. $^{12}_{\Lambda}$B and other p-shell hypernuclei will be measured again with better resolution and higher statistics. The $^{12}_{\Lambda}$B system will serve also as a monitor and for calibrating the new HNSS system.

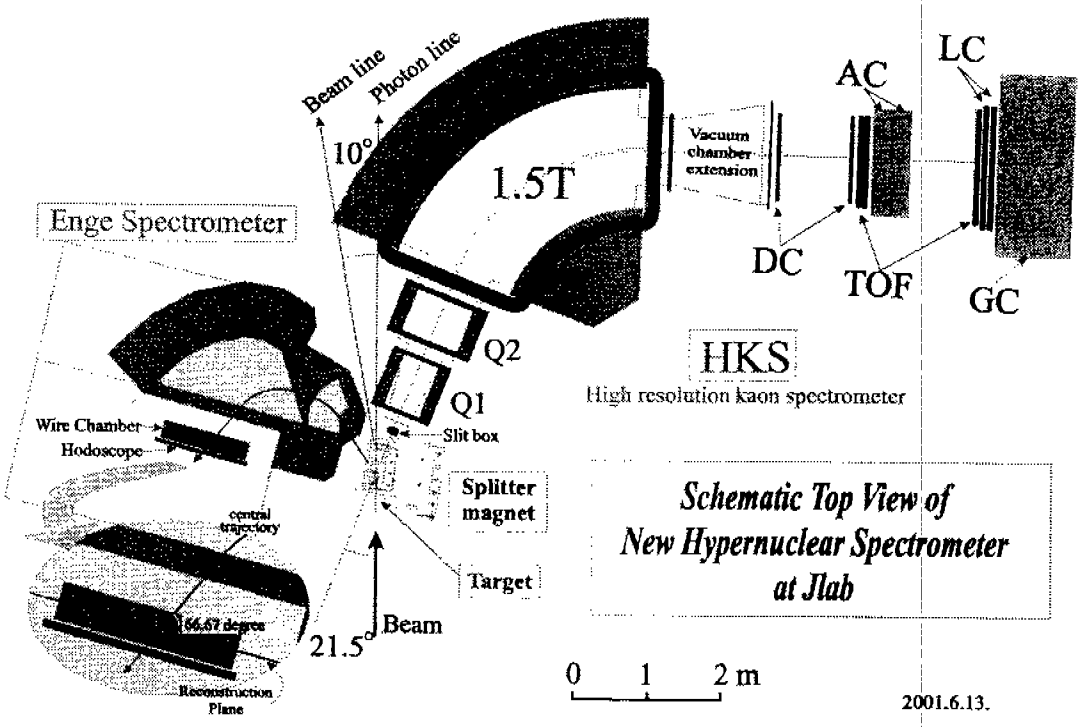

FIGURE 8. Experimental layout of the new HNSS system. The HKS replaces the SOS used in the current experiment.

5. SUMMARY

In the first experiment using the HNSS at JLab, sub-1-MeV energy resolution has been obtained in the spectrum from the $^{12}C(e, e'K^+)^{12}{}_{\Lambda}B$ reaction. The experiment succeeded in spite of an extremely high rate of electrons from bremsstrahlung and demonstrated that electroproduction can be used effectively for hypernuclear spectroscopic studies. Our preliminary spectrum shows strong peaks where spin-flip excitations are expected. Systematic studies of such transitions, produced by the large spin-flip amplitude for the electroproduction of hypernuclei, will complement hypernuclear studies by hadronic probes. The high-quality electron beam at JLab provides new opportunities for future hypernuclear studies. In addition, the new HKS which is currently being constructed and new experimental geometry, will provide a 200-fold increase in good event rates and more than a factor of two improvement in energy resolution.

ACKNOWLEDGMENTS

We acknowledge support by the staff at both the accelerator and physics divisions at the Thomas Jefferson National Accelerator Facility (JLab). L. Tang wishes to thank Dr. D. J. Millener for many useful discussions and for making his most recent

structure predictions available prior to publication. The Southeastern University Research Association (SURA) operates JLab for the U.S. Department of Energy under Contract No. DE-AC05-84ER40150. This work is supported in part by research grants from the U.S. Department of Energy and the National Science Foundation. We would acknowledge the support by the U.S. DOE grants DE-FG02-97ER41047, DE-FG02-87ER40362, and the NSF grant HRD-9633750.

REFERENCES

1. B. F. Gibson and E. V. Hungerford III, *Physics Reports* **257,** 349-388 (1995).
2. C. Milner et al., *Phys. Rev. Lett.* **54,** 1237 (1985).
3. P. H. Pile et al., *Phys. Rev. Lett.* **66,** 2585 (1991).
4. C. B. Dover, *Proc. Int. Symp. on Medium Energy Physics,* Beijing, World Scientific, 1987, p.257.
5. H. Bandō, T. Motoba and Y. Yamamoto, *Phys. Rev.* **C31,** 265 (1985).
6. A. Likar, M. Rosina and B. Povh, *Z. Phys.* **A324,** 35 (1986).
7. A. Gal, *Adv. Nucl. Sci.* **8,** 1 (1977).
8. B. Povh, *Ann. Rev. Nucl. Part. Sci.* **28,** 1 (1978).
9. O. Hashimoto, *Proc. Int. Workshop on Strangeness Nuclear Physics,* Seoul, World Scientific, 1999, p. 116;
   T. Hasegawa et al., *Phys. Rev. Lett.* **74,** 224 (1995);
   T. Hasegawa et al., *Phys. Rev.* **C53**, 1210 (1996);
10. H. Tamura et al., *Phys. Rev. Lett.* **84**, 5963 (2000).
11. K. Tanida et al., *Phys. Rev. Lett.* **86**, 1982 (2001).
12. R. E. Chrien and C. B. Dover, *Ann. Rev. Nucl. Part. Sci.* **39,** 113 (1989).
13. T. W. Donnelly and S. R. Cotanch, *Proceedings of the 1985 CEBAF Summer Study,* 1985;
    C. Hyde-Wright et al., *Proceedings of the 1985 CEBAF Workshop,* 1985;
    S. S. Hsiao and S. R. Cotanch, *Phys Rev.* **C28,** 1668 (1983);
    S. R. Cotanch and S. S. Hsiao, *Nucl. Phys.* **A450,** 419 (1986).
14. T. Motoba, M. Stone and K. Itonaga, *Progress of Theoretical Physics Supplement* **No. 117,** 1994, pp. 123-133; and M. Sotona and S. Frullani, *ibid.,* pp. 151-175.
15. S. Nozawa and T.S. Lee, Nucl. Phys. **A513**, 511 (1990).
16. J. E. Spencer and H. A. Enge, *Nucl. Instr. Meth.* **49**, 177 (1967).
17. D. J. Millener, *private communication.*
18. O. Hashimoto, L. Tang, and J. Reinhold, *E01-011 experimental proposal to JLab PAC 19,* 2001.
19. O. Hashimoto (Spokesperson), *"Specially Promoted Research" of Grant-in-Aid for Scientific Research (2000-2004),* Monkasho, Japan.